



Direct observation of two dimensional trace gas distribution with an airborne Imaging DOAS instrument

K.-P. Heue, T. Wagner, S. P. Broccardo, D. Walter, S. J. Piketh, K. E. Ross, S. Beirle,
U. Platt

► To cite this version:

K.-P. Heue, T. Wagner, S. P. Broccardo, D. Walter, S. J. Piketh, et al.. Direct observation of two dimensional trace gas distribution with an airborne Imaging DOAS instrument. *Atmospheric Chemistry and Physics Discussions*, 2008, 8 (3), pp.11879-11907. <hal-00304268>

HAL Id: hal-00304268

<https://hal.science/hal-00304268v1>

Submitted on 18 Jun 2008

HAL is a multi-disciplinary open access archive for the deposit and dissemination of scientific research documents, whether they are published or not. The documents may come from teaching and research institutions in France or abroad, or from public or private research centers.

L'archive ouverte pluridisciplinaire **HAL**, est destinée au dépôt et à la diffusion de documents scientifiques de niveau recherche, publiés ou non, émanant des établissements d'enseignement et de recherche français ou étrangers, des laboratoires publics ou privés.



HAL Authorization

**Airborne imaging
DOAS**

K.-P. Heue et al.

Direct observation of two dimensional trace gas distribution with an airborne Imaging DOAS instrument

**K.-P. Heue¹, T. Wagner², S. P. Broccardo³, D. Walter¹, S. J. Piketh³, K. E. Ross⁴,
S. Beirle², and U. Platt¹**

¹Institut für Umweltphysik (IUP), Universität Heidelberg, Heidelberg, Germany

²Max Planck Institut für Chemie, Mainz, Germany

³Climatology Research Group, University of the Witwatersrand, Johannesburg, South Africa

⁴Research and Innovation Department, Eskom, South Africa

Received: 26 March 2008 – Accepted: 30 May 2008 – Published: 13 June 2008

Correspondence to: K.-P. Heue (klaus-peter.heue@iup.uni-heidelberg.de)

Published by Copernicus Publications on behalf of the European Geosciences Union.

Title Page

Abstract

Introduction

Conclusions

References

Tables

Figures

◀

▶

◀

▶

Back

Close

Full Screen / Esc

Printer-friendly Version

Interactive Discussion



Abstract

In many investigations of tropospheric chemistry information about the two dimensional distribution of trace gases on a small scale (e.g. tens to hundreds of meters) is highly desirable. An airborne instrument based on imaging Differential Optical Absorption Spectroscopy has been built to map the 2-D distribution of a series of relevant trace gases including NO₂, HCHO, C₂H₂O₂, H₂O, O₄, SO₂, and BrO on a scale of 100 m.

Here we report on the first tests of the novel aircraft instrument over the industrialised South African Highveld, where large variations in NO₂ column densities in the immediate vicinity of several sources e.g. power plants or steel works, were measured.

The observed patterns in the trace gas distribution are interpreted with respect to flux estimates, and it is seen that the fine resolution of the measurements allows separate sources in close proximity to one another to be distinguished.

1 Introduction

Several methods exist to retrieve two dimensional trace gas distributions in the atmosphere on various scales. Satellite observations lead to two dimensional distribution patterns on a global scale; however, the resolution is still rather coarse (several tens of km). On smaller scales (several km) tomographic inversion methods have been applied. The resolution of this method strongly depends on the number of light paths. Therefore a fine resolution can only be achieved by installing a large number of instruments (Hartl et al., 2006). With the new airborne imaging Differential Optical Absorption Spectrometer (iDOAS), trace gas distributions can be observed directly at a resolution of less than 100 m. The main species to be observed with iDOAS are NO₂, HCHO, C₂H₂O₂, H₂O, O₄, SO₂, and BrO. Based on the observed patterns, sources and sinks can be quantified and chemical processes including conversion rates and atmospheric lifetimes may be analysed.

The BrO formation in volcanic plumes has been studied using ground-based iDOAS

ACPD

8, 11879–11907, 2008

Airborne imaging DOAS

K.-P. Heue et al.

Title Page

Abstract

Introduction

Conclusions

References

Tables

Figures

◀

▶

◀

▶

Back

Close

Full Screen / Esc

Printer-friendly Version

Interactive Discussion



measurements (Bobrowski et al., 2007). On larger scales satellite data have been used to quantify the strength of ship emissions based on the SCIAMACHY NO₂ distribution patterns in the Indian Ocean (Beirle et al., 2004).

Due to the high spatial resolution of the airborne iDOAS instrument, independent sources located within small distances of one another may be resolved and quantified separately. The results can be used for satellite and chemical transport model validation. The variability within a satellite pixel is one of the major issues to be addressed with the imaging DOAS instrument.

Results of tests of the iDOAS over the South African interior plateau, called the Highveld, are reported in this paper. The Highveld is the most highly industrialised region in southern Africa (Fig. 1), and satellite-detected NO₂ column densities over the Highveld are the highest in the Southern Hemisphere and equivalent to those in the highly industrialised regions of east Asia, the Middle East, Europe and North America (Beirle et al., 2006). Large power plants, synfuels refinery, metallurgical smelters, industries, mines and urban conglomerations on the Highveld are large area and point sources of pollution. Stable atmospheric conditions in the region favour plumes to remain intact at large distances downwind of the sources. The Highveld is an ideal location to test the operation of a high resolution instrument like the airborne iDOAS

2 The measurement technique

The imaging DOAS technique was previously used in ground based applications (Lohberger et al., 2004; Bobrowski et al., 2007) to map the trace gas distribution resulting from stack or volcano emissions. For that purpose the instrument was directed towards the interesting object (Fig. 2). One section or column of the scene is imaged on the entrance slit of the spectrograph. The reflected and scattered sunlight is spectrally dispersed and recorded by a charge-coupled device (CCD). Each individual line of the CCD chip corresponds to a spectrum and using the DOAS technique (Sect. 2.3) results in one trace gas slant column density.

Airborne imaging DOAS

K.-P. Heue et al.

Title Page

Abstract

Introduction

Conclusions

References

Tables

Figures

◀

▶

◀

▶

Back

Close

Full Screen / Esc

Printer-friendly Version

Interactive Discussion



The DOAS analysis yields a slant column density (SCD) which is the integrated concentration along the light path (Sect. 2.3). In such a way, one section (column) of the respective trace gas distribution is observed. To obtain the two dimensional distribution of the slant column densities the instrument scans the scene perpendicular to the entrance slit (Fig. 2). In this study the results are mainly expressed as slant column densities. They can be colour coded to illustrate the trace gas patterns.

2.1 Instrumental setup

The imaging DOAS instrument consists of an imaging spectrograph and a two dimensional detector i.e. a CCD camera. An optical system in front of the spectrograph focuses the incoming radiance onto the entrance slit. A large field of view (5–60°) is mapped on the spectrograph. The height h of the entrance slit and the focal length f of the entrance optics determine the field of view γ :

$$\tan(\gamma/2) = \frac{h}{2 \cdot f} \quad (1)$$

The light entering the spectrograph is spectrally analysed and detected by the CCD. The DOAS analysis of the recorded spectra yields one column of trace gas information.

The instrument is installed on the aircraft with the entrance slit perpendicular to the flight direction. As the entrance optics generates a swath perpendicular to the flight direction, this technique is called push broom imaging. The principle is illustrated in Fig. 3.

The aeroplane moves forward as a column of trace gas information is being recorded; the resolution parallel to the flight direction is determined by the speed of the aircraft and the exposure time. After data from the CCD has been read out the next set of spectra is recorded. In the mean time the trace gas contribution below the plane may have changed. In such a way, information about the two dimensional trace gas distributions below the aeroplane can be gained.

Title Page

Abstract

Introduction

Conclusions

References

Tables

Figures

◀

▶

◀

▶

Back

Close

Full Screen / Esc

Printer-friendly Version

Interactive Discussion



The resolution perpendicular to the flight direction is determined by the magnification of the optical system and the numbers of lines on the CCD chip i.e. 255 for our instrument. However due to the imperfect imaging qualities of the system (Sect. 2.2) 8 lines have to be co-added, thus reducing the resolution to 32 lines perpendicular to the flight direction. Moreover the signal to noise ratio is improved, and the detection limit reduced, when several CCD lines are co-added.

The instrumentation used for this study consists of an ACTON 300i imaging spectrograph, which is a Czerny-Turner type with 300 mm focal length, an Andor DU-420BU CCD with 255 x 1024 pixel, and a mirror based entrance optics.

Details of the optical system are illustrated in Fig. 4. The first mirror is convex with a focal length of 51.5 mm and the second one is concave and has 25.6 mm focal length. The combination of both placed 70 mm apart results in the focal length of 13.7 mm. As the entrance slit is 6.9 mm high, according to Eq. (1) the total field of view is 28° and the total field of view equals half the flight altitude above ground. As the sensitivity of the DOAS measurement strongly depends on the length of the light path through the trace gas distribution, one might think that it would be more sensitive towards the edges of the images. However if the geometrical light path at the edges is compared to the nadir (centre), it is enhanced by $1/\cos(14^\circ)=1.03$ i.e. only 3%.

In contrast to the ideal setup illustrated in Fig. 4, the optical window in the aeroplane was a little bit too small, reducing the field of view to 24° . Each swath was divided into 27 ground pixels instead of 32. Assuming a standard flight altitude of 4500 m above ground level (a.g.l), the total swath was 1910 m wide and the lateral resolution was 71 m.

2.2 Characterisation of the instrument

To characterise the imaging quality of the instruments several tests with different light sources were performed. Most artificial light sources had to be installed rather close to the instrument, hence the optical system tests was slightly different to the real measurements. One of the most convincing tests was to setup the instrument inside the

Airborne imaging DOAS

K.-P. Heue et al.

Title Page

Abstract

Introduction

Conclusions

References

Tables

Figures

◀

▶

◀

▶

Back

Close

Full Screen / Esc

Printer-friendly Version

Interactive Discussion



hangar and direct it towards the doors. Each of the four doors was 4.5 m wide and the distance to the instrument was 19 m. If the doors were opened by 30 cm, it resulted in three vertically extended light sources of 30 cm width separated by 4.5 m at a distance of 19 m from the instrument (Fig. 5). The instrument's total field of view is 9.5 m wide at the doors position.

A light source of 30 cm width at a distance of 19 m is expected to result in a spectrum of 255 pixels/9.5 m·0.3 m≈8 pixels on the CCD. The observed image is shown in Fig. 6. The central spectrum has a full width of half maximum (FWHM) of 8 pixels. If the light source was made smaller (by closing the doors slightly) only a small decrease was observed, whereas if the doors were opened a clear increase in the width of the spectra was visible. Therefore the minimum resolution of the complete system is approximately 8 pixels or 0.8°.

The minimum resolution along the flight direction is also determined by the optical system. If the motion of the plane is ignored or integration time is infinitely small, the instantaneous resolution would be 11 m at a flight altitude of 4500 m a.g.l. This has to be added to the distance the plane travels during the actual integration time. In total the typical resolution ranges between 90 m and 200 m. A small gap (29 m) between the individual scans was caused by the CCD readout procedure, which lasted 0.4 s. The width of the gap also depends on the flight altitude; if the plane is flying low the gap is bigger, as the minimum resolution gets finer (Fig. 10).

The iDOAS instrument was installed on the Rockwell Aerocommander 690A operated by the South African Weather Service (ZS-JRA). The standard flight altitude was 6 km AMSL or 4.5 km a.g.l.; the speed ranged from 95 m/s to 135 m/s. The typical integration time was about 1 seconds or less, hence the spatial resolution in the flight direction is about 100 m.

The exact instrument's field of view relative to the aeroplane is very hard to determine, therefore the viewing direction is a bit uncertain, even if the exact roll and pitch angles were available. The total signal of the recorded light intensity divided by the integration time gives us a black and white image of the local surrounding

**Airborne imaging
DOAS**

K.-P. Heue et al.

Title Page

Abstract

Introduction

Conclusions

References

Tables

Figures

◀

▶

◀

▶

Back

Close

Full Screen / Esc

Printer-friendly Version

Interactive Discussion



which can be compared to more precise satellite images e.g. Google Earth images <http://earth.google.com>.

2.3 DOAS Technique

To retrieve column densities from the observed spectra, the well known DOAS technique (Platt, 1994) is applied. The method is based on Lambert-Beer's law.

The absorption cross section (σ) is a characteristic function of the wavelength λ for the individual trace gases. The integrated concentration along the light path is called slant column density and is the result of the DOAS analysis. A normal in-flight spectrum in a remote and clean area is usually taken as the reference here. Thereby the Fraunhofer structures are removed from the fit and the stratospheric background concentration is subtracted. However if the remote region is not as clear as expected, parts of the tropospheric signal are subtracted as well. Hence the results presented in Sect. 3 constitute lower limits of true tropospheric SCDs, they are usually referred to as differential slant column densities.

The wavelength range between 467 and 517 nm was chosen for the analysis and, besides NO₂, (Vandaele et al., 1997) the cross sections of water vapour (Rothman et al., 1998), O₄ (Hermans et al., 1999) and O₃ (Burrows et al., 1999) were included. The filling in of the Fraunhofer lines due to inelastic Raman scattering (Ring effect) (Grainer and Ring, 1962) was considered by using an appropriate cross section (Gomer et al., 1996). The instrumental function varies across the CCD chip in both dimensions. Therefore individual reference and ring spectra are applied in the fit for the spectra recorded in the respective regions of the CCD-chip. Moreover an individual calibration was used for each line. For the central CCD line a NO₂ fit is shown in Fig. 7. The spectrum was recorded on 5 October 2006 close to the synthetic oil refinery in Secunda (Fig. 8 and 9).

The retrieved data is equivalent to the integrated concentration along the light path - the SCD. The tropospheric vertical column density (tvCD) is often a more accurate quantity for further analysis. It gives the integrated concentration across the altitude

Airborne imaging DOAS

K.-P. Heue et al.

Title Page

Abstract

Introduction

Conclusions

References

Tables

Figures

◀

▶

◀

▶

Back

Close

Full Screen / Esc

Printer-friendly Version

Interactive Discussion



up to the mixing layer height and is therefore independent of the light path. The ratio between slant and vertical column is called the air mass factor (AMF). It has to be simulated in a radiative transfer model. The complete light path between the instrument and the sun has to be considered for the model calculation. In this case the Monte Carlo-based radiative transfer model TRACY (Wagner et al., 2007; Deutschmann and Wanger, 2007) was used. The geometry of the setup including solar zenith angle was considered and the terrain altitude (1600 m) was included. The altitude is not quite correct for the entire Highveld, but within a range of 200 m no altitude dependency was observed in the simulation. Especially in dense plumes, aerosols can reduce the visibility; however, this effect was completely ignored here, as no significant change in the O_4 observation was detected. Due to emissions of water vapour clouds sometimes can be observed above power plants. This was not the case in the dry season on the Highveld. As the AMF calculation showed no strong variation between the different parts of the image, a constant AMF of 2.2 is used independent of the viewing direction. Most of the presented data are slant column densities. The flux estimate in Sect. 3.3 is the only result where an AMF was applied.

3 Results

3.1 First measurement

Three test flights over large pollution sources (coal-fired power plants, steel works and refineries) on the Highveld were flown on 4, 5 and 6 October 2006. The NO_2 column densities showed strong gradients in the immediate vicinity of various sources. An overview of the flight track from the first and the second flight (4 and 5 October 2006) is shown in Fig. 8. The flight track and the observed NO_2 column densities of the third flight are compared to SCIAMACHY data in Fig. 14. Enhanced NO_2 column densities are observed downwind of the plants. Here only the nadir direction (CCD-line 16) and no gradients in the column densities perpendicular to the flight direction are shown.

Title Page

Abstract

Introduction

Conclusions

References

Tables

Figures

◀

▶

◀

▶

Back

Close

Full Screen / Esc

Printer-friendly Version

Interactive Discussion



During the 2nd flight the plume from Kendal power station was observed to merge with the plumes from Matla and Kriel power stations to form one large plume which broadened with distance downwind. The plume of the synfuels refinery in Secunda was crossed three times at different distances downwind of the plant. The plume from the refinery is also observed to broaden and become more diffuse with distance from the source.

3.2 Two dimensional NO₂ distributions

Detailed 2-D images of the NO₂ SCD close to selected sources are shown in Figs. 9, 10 and 11.

In Fig. 9 the mixing of NO₂ plumes originating from different sources in Secunda is visible. Both plumes extend in different directions, which allows a qualitative altitude determination.

While the large plume seems to be close to the ground, according to the Eckmann spiral of wind direction the smaller one expands more perpendicular to the flight altitude and can therefore be expected to be at higher levels.

The spatial resolution at ground level theoretically increases when the flight altitude is lower. However, most of the point sources observed here do not emit the respective trace gases at ground level but at 250 m altitude. As the exit temperature of the emitted gases is usually quite high (on the order of 130°C for coal-fired power stations), effective stack height is several hundred metres above actual stack height, and there is a risk of missing the plume or observing only parts of it when flying at lower altitudes.

On 4 October 2007 the aircraft flew over Lethabo power plant in the Vereeniging area south of Johannesburg at 600 m a.g.l. (stack height 275 m; Fig. 10). The local enhancement in NO₂ column densities is observed in only a few pixels. Just north of the plant high intensity of reflected light (probably caused by the cooling tower or the saturated plume above it) led to a blooming effect on the CCD, therefore no valid observation was made here. Although the plume was observed directly beneath the aeroplane and partly downwind, no widening of the plume perpendicular to the wind

Title Page

Abstract

Introduction

Conclusions

References

Tables

Figures

◀

▶

◀

▶

Back

Close

Full Screen / Esc

Printer-friendly Version

Interactive Discussion



direction is observed. The plume broadens by less than one pixel ($\approx 100\text{m}$) at 150m downwind of the stack, or it widens above the flight level and the effect cannot be observed by the downward looking imaging DOAS. Nevertheless the high resolution of 10 m perpendicular to the flight direction is still astonishingly good.

5 A typical plume expansion is observed close to the Majuba power plant (Fig. 11 top). The image is overlaid in Fig. 11 (bottom) to a local satellite image (Google Earth). A strong enhancement in the NO_2 column is observed close to the stack. This is probably caused by the long absorption path when looking on a rising plume from above. Further downwind the plume widens and the local column densities decrease as the plume
10 turns from vertical to horizontal. The local enhancement at the downwind edge of the image is not yet fully understood but seems to be a real change in the slant column density. It may be caused by the oxidation of NO to NO_2 in the plume driven by the mixing in of O_3 . Nitrogen oxides are mostly emitted as NO rather than NO_2 , typically 95% is NO. By reaction with O_3 it converts to NO_2 until the well known Leighton ratio
15 establishes.

If the plume expands in vertical waves, this might again result in a locally extended absorption path through the plume. As the increase in the column density is higher than 3% the observation is not caused by the systematic difference in the sensitivity (Sect. 2.1).

20 The position of the stack in Fig. 11 is determined based on the method described in Sect. 2.2.

3.3 Flux estimate

For the following flux estimate an AMF of 2.2 was applied to the SCD illustrated in Fig. 11. To correct for a slightly enhanced background, the averaged column densities
25 downwind of the power plant (first 8 lines of the image) were subtracted.

For selected distances downwind of Majuba the cross section of the vertical column densities are illustrated in Fig. 12. The maximum of the column density is observed close to the stacks as mentioned above. The maximum flux (Fig. 13) however, is

Airborne imaging DOAS

K.-P. Heue et al.

Title Page

Abstract

Introduction

Conclusions

References

Tables

Figures

◀

▶

◀

▶

Back

Close

Full Screen / Esc

Printer-friendly Version

Interactive Discussion



further downwind when the plume is wider.

After these preparations the flux was estimated by integrating the vertical column densities VCD along the local flight track (x-direction in Eq. 2) considering the local wind speed v_{wind} and wind direction $\alpha_{\text{wind}}^{\text{flightdirection}}$ relative to flight direction:

$$\Phi = \int \text{VCD}(x) \cdot x \cdot v_{\text{wind}} \cdot \sin(\alpha_{\text{wind}}^{\text{flightdirection}}) \cdot dx \quad (2)$$

The wind speed was not measured on board the plane but hourly averaged ground based observations are available in Majuba. The wind on this day 5 October 2006 was rather calm and blew with approximately 2.2 m/s from north western directions ($\approx 296^\circ$) between 10:00 and 12:00 UTC. The observed NO_2 pattern (Fig. 11) however, indicates the wind direction was more from the north $\approx 330^\circ$. The temporal variation in a 5 min interval can not be resolved by hourly averaged data, therefore during the measurements a northern wind direction does not contradict the measured wind direction in Majuba. Due to the high uncertainties in both methods the average wind direction (313°) is considered in the flux estimates.

Downwind of the source a linear increase in the total NO_2 flux is observed (Fig. 13). This of course does not necessarily indicate that additional sources are observed downwind, but it mainly results from the above mentioned NO oxidation and a parallel O_3 destruction.

Upwind of the source the flux is not zero. This might be caused by turbulent mixing near the buildings. It might also be caused by an insufficient background correction, although the flux further away from the plume is far less. Instrumental effects should also not be neglected here. The exact direction in which the instrument is pointed cannot be determined; therefore the position of the enhanced NO_2 columns relative to the real source might be shifted. As the resolution of the IDOAS instrument is quite good the observed increase cannot be explained by a sampling effect.

Title Page

Abstract

Introduction

Conclusions

References

Tables

Figures

◀

▶

◀

▶

Back

Close

Full Screen / Esc

Printer-friendly Version

Interactive Discussion



3.4 Comparison with SCIAMACHY

A first comparison of the iDOAS measurements with SCIAMACHY tropospheric slant columns is shown for the flight on 7 October 2006 in Fig. 14. The finer resolution iDOAS data can be averaged perpendicular to the flight direction for comparison with the satellite instrument.

South of Johannesburg in the industrial region around Vereeniging high column densities were observed. The enhanced local concentrations also lead to an increase in the SCIAMACHY NO₂ data. The large field of view of SCIAMACHY however, is dominated by the low column densities outside the industrial areas. Hence we can estimate the NO₂ variability inside one SCIAMACHY pixel to be rather high, as the enhancement seems to be caused by high column densities in a small area, whereas the surrounding areas seems to be much cleaner.

For the detailed interpretation the temporal mismatch has to be considered. The aeroplane arrived at Sasolburg at 09:55 and returned at 11:25 UTC. ENVISAT (SCIAMACHY) crossed the same area 2 h previously at 07:46 UT. Within these 2 morning hours the atmospheric conditions might have changed significantly.

4 Conclusions

We presented the first direct observations of two dimensional NO₂ distributions over the industrialised Highveld in South Africa. Based on the observed NO₂ patterns two different sources in close proximity to one another can be distinguished, and qualitative altitude determination can be made.

NO₂ flux estimates are possible on the basis of vertical columns and the wind data. Although the maximum column density partly decreases with distant to the stack, an overall increase in the NO₂ flux is observed. Both the widening of the plume and the NO to NO₂ conversion attribute to this effect. A radiative transfer model was used for the calculation of air mass factors; however, some geometrical effects like a localised

Airborne imaging DOAS

K.-P. Heue et al.

Title Page

Abstract

Introduction

Conclusions

References

Tables

Figures

◀

▶

◀

▶

Back

Close

Full Screen / Esc

Printer-friendly Version

Interactive Discussion



plume have not yet been considered. These data could also be compared to data provided by the plant operators.

Slant column densities were compared to satellite data (SCIAMACHY). Although the different spatial resolution of satellite instruments results in large discrepancies between finer resolution iDOAS measurements and coarser resolution satellite measurements (Heue et al., 2005), detailed knowledge about the local distribution inside the satellite pixels is of great interest. For a more quantitative comparison special flights have to be performed, during which the flight is coordinated with satellite overpass time.

To improve the pointing accuracy of the iDOAS, a digital camera will be installed next to the spectrometer. This will give additional information on the area over which the flight is conducted.

The actual wavelength range of the instrument is optimised for NO₂, but several interesting trace gases e.g. SO₂ and HCHO show strong absorption bands in the UV (300–400 nm). Future measurement flights will use a slightly different instrument optimised for the observation of these trace gases as well.

Additional measurement flights in the Highveld (South Africa) were performed in August 2007 and March 2008, in order to validate the satellite retrievals on a regional scale and investigate individual sources on a local scale. The analysis of this data is still in progress.

Acknowledgements. Financial support for this research project was provided by Eskom Corporate Services as part of their Research and Development Programme and is gratefully given credits. Thanks to the South African Weather Service for the support of the aeroplane and the logistical support in Bethlehem, including the daily weather briefing.

References

Bobrowski, N., Glasow, R.v., Aiuppa, A., Inguaggiato, S., Louban, I., Ibrahim, O. W., and Platt, U.: Reactive Halogen Chemistry in Volcanic Plumes, J. Geophys. Res., 112, D06311,

Airborne imaging DOAS

K.-P. Heue et al.

Title Page

Abstract

Introduction

Conclusions

References

Tables

Figures

◀

▶

◀

▶

Back

Close

Full Screen / Esc

Printer-friendly Version

Interactive Discussion



doi:10.1029/2006JD007206, 2007. [11881](#)

Beirle, S., Platt, U., von Glasow, R., Wenig, M., and Wagner, T.: Estimate of nitrogen oxide emission from shipping by satellite remote sensing, *Geophys. Res. Lett.*, 31, L18102, doi:10.1029/2004GL020312, 2004. [11881](#)

5 Beirle, S., Platt, U., and Wagner, T.: Potential of monitoring nitrogen oxides with satellite instruments, *Proceeding of The 2006 EUMETSAT Meteorological Satellite Conference*, Helsinki, Finland, http://www.eumetsat.int/Home/Main/Publications/Conference_and_Workshop_Proceedings/groups/cps/documents/document/pdf_conf_p48_s4_02_beirle_v.pdf 12–16 June 2006, last access: 3 June 2008. [11881](#), [11894](#), [11907](#)

10 Burrows, J. P., Richter, A., Dehn, A., Deters, B., Himmelmann, S., Voigt, S., and Orphal, J.: Atmospheric remote-sensing reference data from GOME: Part 2. Temperature-dependent absorption cross-sections of O₃ in the 231–794 nm range, *J. Quant. Spectrosc. Ra.*, 61, 509–517, 1999. [11885](#)

Deutschmann, T. and Wagner, T.: *Tracy User manual*, Universität Heidelberg, 2007. [11886](#)

15 Grainger, J. and Ring, J.: Anomalous Fraunhofer line profiles, *Nature*, 193, 762, 1962. [11885](#)

Gomer, T., Brauers, T., Heintz, F., Stutz, J., and Platt, U.: *MFC 1.98 m User Manual*. Institut für Umweltphysik, 1996. [11885](#)

Hartl, A., Song, B. C., and Pundt, I.: 2-D reconstruction of atmospheric concentration peaks from horizontal long path DOAS tomographic measurements: parametrisation and geometry within a discrete approach, *Atmos. Chem. Phys.*, 6, 847–861, 2006, <http://www.atmos-chem-phys.net/6/847/2006/>. [11880](#)

Heue, K.-P., Richter, A., Bruns, M., Burrows, J. P., Friedeburg, C. v., Platt, U., Pundt, I., Wang, P. and Wagner, T., Validation of SCIAMACHY tropospheric NO₂-columns with AMAXDOAS measurements, *Atmos. Chem. Phys.*, 5, 1039–1051, 2005, <http://www.atmos-chem-phys.net/5/1039/2005/>. [11891](#)

25 Heue, K.-P., Wagner, T., Broccardo, S. P., Piketh, S. J., Ross, K. E., and Platt, U.: Direct Observation of two dimensional trace gas distribution with an airborne Imaging DOAS instrument, *Proceedings of the ESA Conference on Rockets and Balloons and related research*, 4th–7th June 2007, Visby, Sweden, 2007. [11902](#)

30 Hermans, C., Vandaele, A. C., Carleer, M., Fally, S., Colin, R., Jenouvrier, A., Coquart, B. and Mrienne, M. F.: Absorption-cross sections of atmospheric constituents: NO₂, O₂ and H₂O, *Environ. Sci. Pollut. Res.*, 6, 3, 151–158, 1999. [11885](#)

Lohberger, F., Hönninger, G., and Platt, U.: Ground-based imaging differential optical absorp-

Airborne imaging DOAS

K.-P. Heue et al.

Title Page

Abstract

Introduction

Conclusions

References

Tables

Figures

◀

▶

◀

▶

Back

Close

Full Screen / Esc

Printer-friendly Version

Interactive Discussion



tion spectroscopy of atmospheric gases, Appl. Optics, 43, 24, 4711–4717, 2004. 11881, 11895

Rothman, L. S.: The HITRAN molecular spectroscopic database and HAWKS (HITRAN Atmospheric Workstation): 1996 edition, J. Quant. Spectrosc. Ra., 60, 5, 665–710, 1998. 11885

5 Platt, U.: Differential Optical Absorbtion Spectroscopy (DOAS), in: Monitoring by spectroscopic techniques, edited by: Sigrist, M. W., New York: John Wiley & Sons, Inc, 1994. 11885

Vandaele, A. C., Hermans, C., Simon, P. C., Carleer, M., Colin, R., Fally, S., Mrienne, M.-F., Jenouvrier, A., and Coquart, B.: Measurements of the NO₂ Absorption Cross-section from 42 000 cm⁻¹ to 10 000 cm⁻¹ (238–1000 nm) at 220 K and 294 K, J. Quant. Spectrosc. Ra., 10 59, 171–184, 1997. 11885

Wagner, T., Burrows, J. P., Deutschmann, T., Dix, B., von Friedeburg, C., Frieß, U., Hendrick, F., Heue, K.-P., Irie, H., Iwabuchi, H., Kanaya, Y., Keller, J., McLinden, C. A., Oetjen, H., Palazzi, E., Petritoli, A., Platt, U., Postlyakov, O., Pukite, J., Richter, A., van Roozendaal, M., Rozanov, A., Rozanov, V., Sinreich, R., Sanghavi, S., and Wittrock, F.: Comparison of box-air-mass-factors and radiances for Multiple-Axis Differential Optical Absorption Spectroscopy (MAX-DOAS) geometries calculated from different UV/visible radiative transfer models, Atmos. Chem. Phys., 7, 1809–1833, 2007, <http://www.atmos-chem-phys.net/7/1809/2007/>. 11886

ACPD

8, 11879–11907, 2008

Airborne imaging DOAS

K.-P. Heue et al.

Title Page

Abstract

Introduction

Conclusions

References

Tables

Figures

◀

▶

◀

▶

Back

Close

Full Screen / Esc

Printer-friendly Version

Interactive Discussion



**Airborne imaging
DOAS**

K.-P. Heue et al.

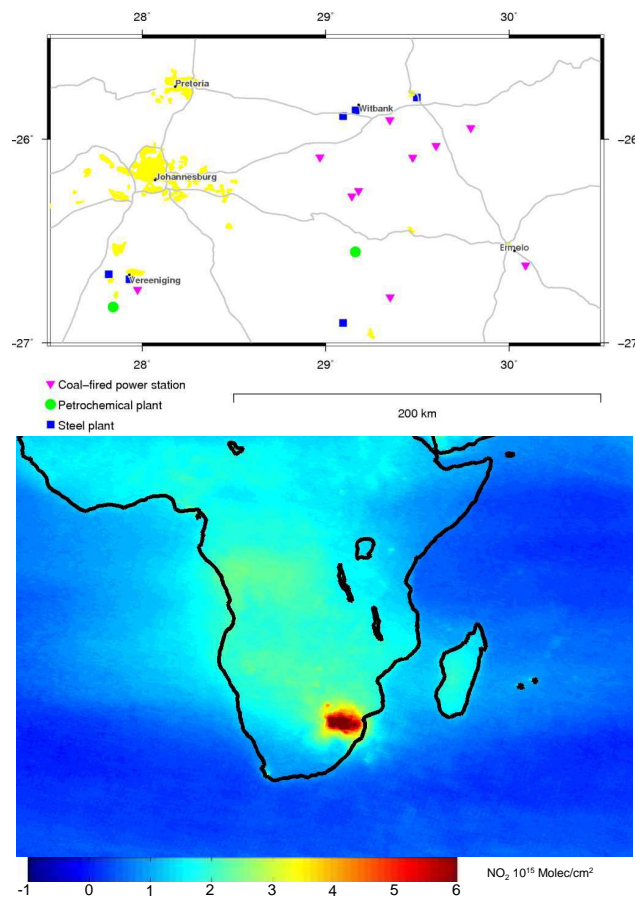


Fig. 1. Map of the Heighveld including the position of the main industries. Averaged tropospheric NO₂ column from SCIAMACHY measurements 2003–2006 (Beirle et al., 2006).

Title Page

Abstract

Introduction

Conclusions

References

Tables

Figures

I◀

▶I

◀

▶

Back

Close

Full Screen / Esc

Printer-friendly Version

Interactive Discussion



**Airborne imaging
DOAS**

K.-P. Heue et al.

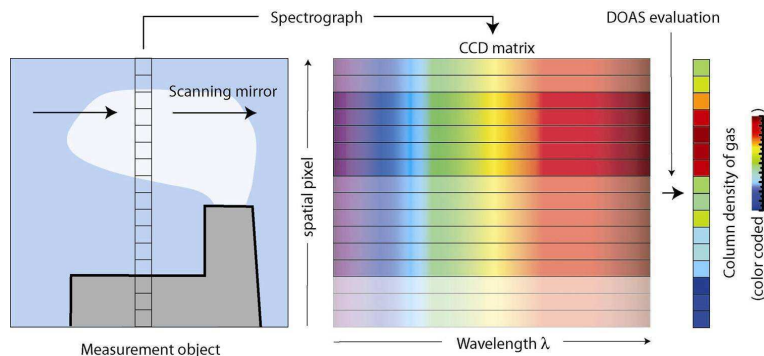
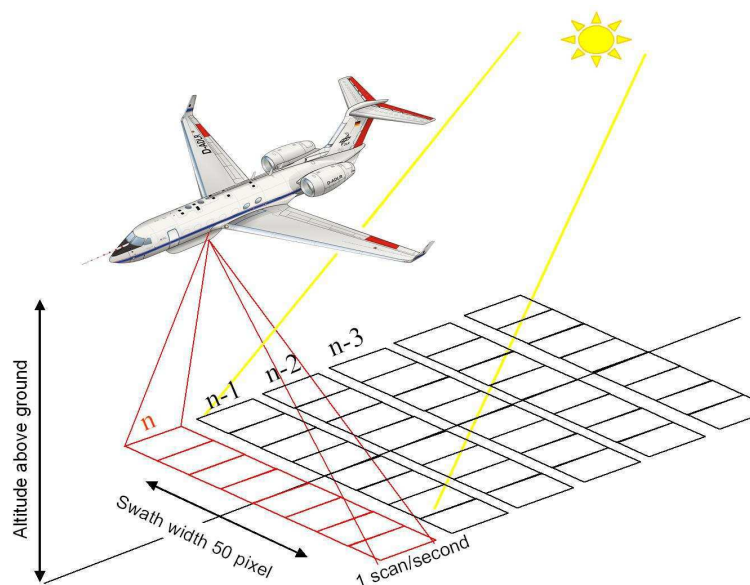


Fig. 2. Principle of the imaging DOAS technique (Lohberger et al., 2004).

[Title Page](#)[Abstract](#)[Introduction](#)[Conclusions](#)[References](#)[Tables](#)[Figures](#)[I◀](#)[▶I](#)[◀](#)[▶](#)[Back](#)[Close](#)[Full Screen / Esc](#)[Printer-friendly Version](#)[Interactive Discussion](#)

**Airborne imaging
DOAS**

K.-P. Heue et al.

**Fig. 3.** Sketch of the airborne iDOAS technique.[Title Page](#)[Abstract](#)[Introduction](#)[Conclusions](#)[References](#)[Tables](#)[Figures](#)[I◀](#)[▶I](#)[◀](#)[▶](#)[Back](#)[Close](#)[Full Screen / Esc](#)[Printer-friendly Version](#)[Interactive Discussion](#)

**Airborne imaging
DOAS**

K.-P. Heue et al.

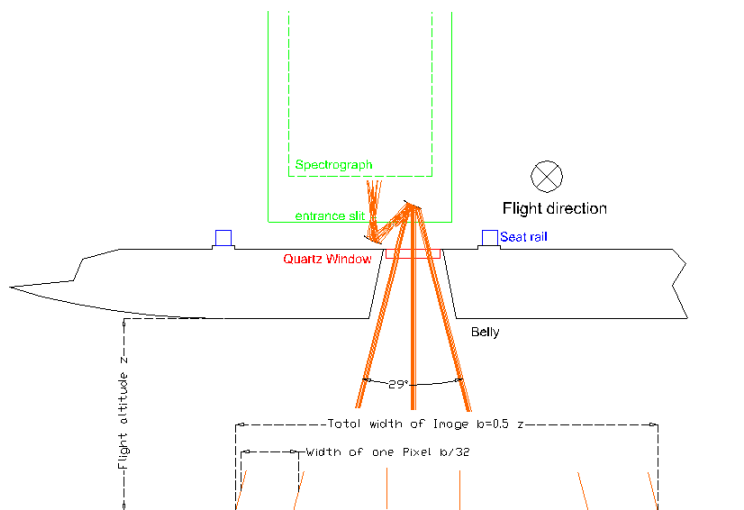


Fig. 4. Details of the mirror based entrance optics looking from the back of the aircraft. The total swath width equals half the flight altitude and is divided into 32 pixels. Due to obstruction from the belly only 27 pixels receive a significant signal.

[Title Page](#)[Abstract](#)[Introduction](#)[Conclusions](#)[References](#)[Tables](#)[Figures](#)[I◀](#)[▶I](#)[◀](#)[▶](#)[Back](#)[Close](#)[Full Screen / Esc](#)[Printer-friendly Version](#)[Interactive Discussion](#)

**Airborne imaging
DOAS**

K.-P. Heue et al.

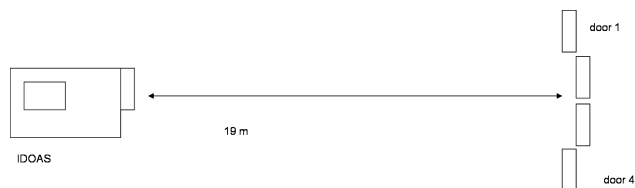


Fig. 5. Ground setup used to characterise the optical properties of the airborne iDOAS. Each hangar door was 4.5 m wide and the small openings in between were 30 cm, hence the total distance between the light sources was 9.9 m (edge to edge).

Title Page

Abstract

Introduction

Conclusions

References

Tables

Figures

I◀

▶I

◀

▶

Back

Close

Full Screen / Esc

Printer-friendly Version

Interactive Discussion



**Airborne imaging
DOAS**

K.-P. Heue et al.

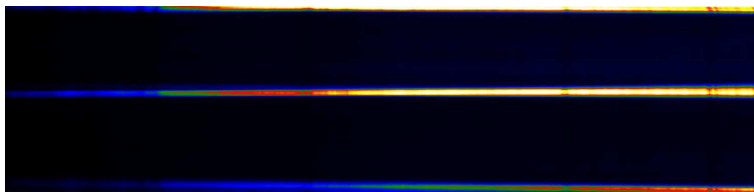


Fig. 6. CCD image of the three hangar doors. Only parts of the outermost slits are observed. This is expected as the distance between the doors and the instrument is less than double the distance between light sources. The total chip is 255 lines wide and the illuminated area in the centre covers 8 lines.

[Title Page](#)[Abstract](#)[Introduction](#)[Conclusions](#)[References](#)[Tables](#)[Figures](#)[I◀](#)[▶I](#)[◀](#)[▶](#)[Back](#)[Close](#)[Full Screen / Esc](#)[Printer-friendly Version](#)[Interactive Discussion](#)

**Airborne imaging
DOAS**

K.-P. Heue et al.

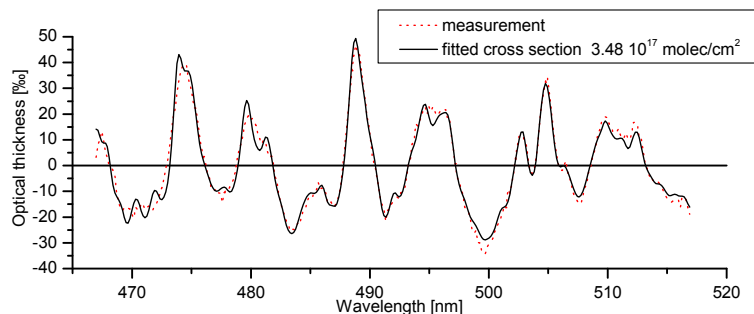


Fig. 7. Example fit of the DOAS Analysis for NO_2 . The analyzed spectrum was observed on 5 October 2006 downwind of Secunda synfuel refinery (spectrum 1355 line 16).

[Title Page](#)[Abstract](#)[Introduction](#)[Conclusions](#)[References](#)[Tables](#)[Figures](#)[◀](#)[▶](#)[◀](#)[▶](#)[Back](#)[Close](#)[Full Screen / Esc](#)[Printer-friendly Version](#)[Interactive Discussion](#)

Airborne imaging
DOAS

K.-P. Heue et al.

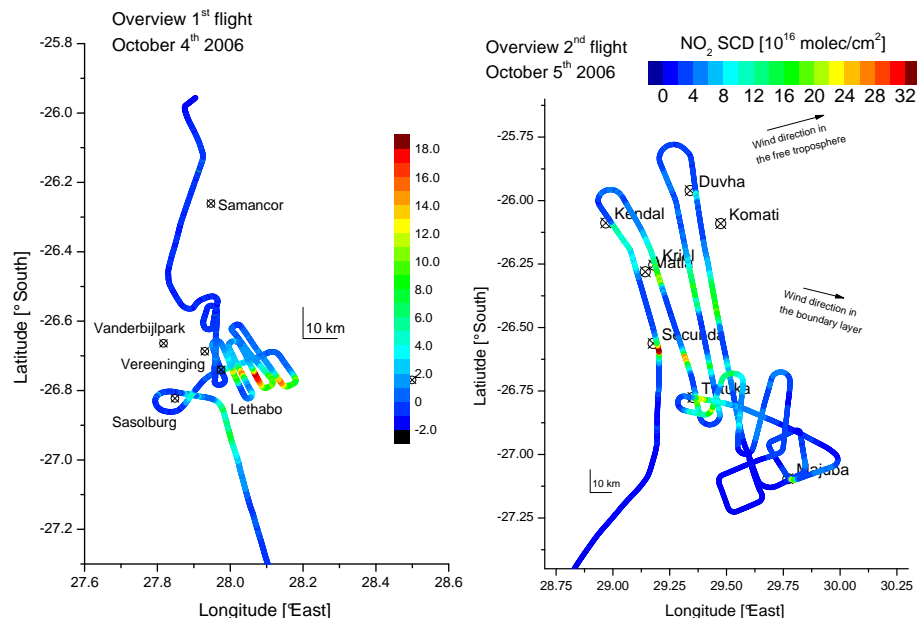


Fig. 8. Overview of the tracks of the flight on 4 and 5 October 2006 close to pollution sources. The tracks are colour coded to indicate the NO₂ slant column density in nadir.

Title Page

Abstract

Introduction

Conclusions

References

Tables

Figures

I◀

▶I

◀

▶

Back

Close

Full Screen / Esc

Printer-friendly Version

Interactive Discussion



Airborne imaging
DOAS

K.-P. Heue et al.

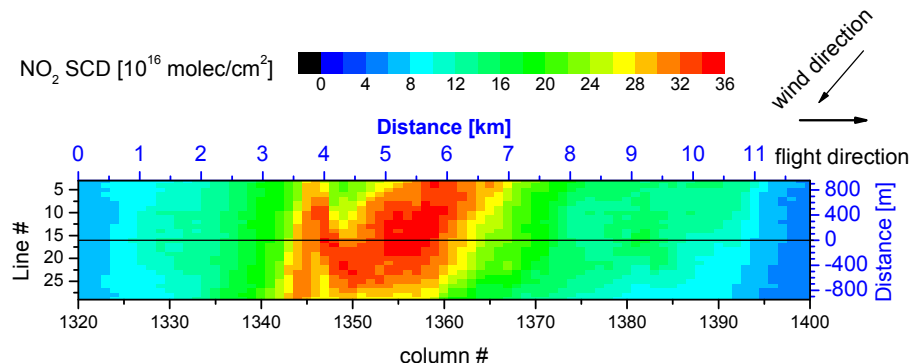


Fig. 9. NO₂ SCD close to the synthetic fuel refinery in Secunda, showing the mixing of two plumes (Heue et al., 2007). Both plumes probably originate from the refinery but from different sources, however they can clearly be resolved. The gaps (Fig. 10) between the individual columns are not shown as they are rather small due to the flight altitude

Title Page

Abstract

Introduction

Conclusions

References

Tables

Figures

I◀

▶I

◀

▶

Back

Close

Full Screen / Esc

Printer-friendly Version

Interactive Discussion



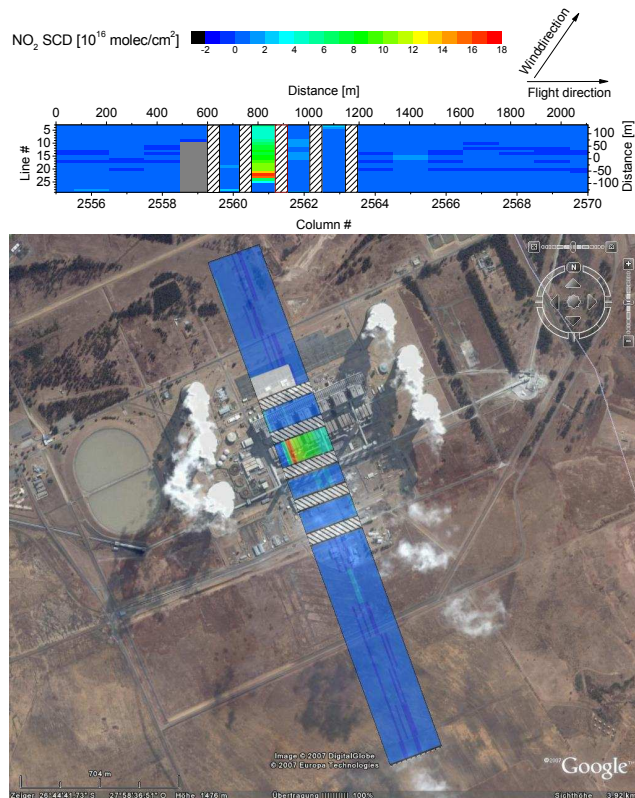


Fig. 10. Enhanced NO₂ SCDs over the stack of Lethabo power station 4 October 2006. The CCD was partly oversaturated leading to a blooming effect; hence no data are shown just north of the plant. No spectra are observed during the read out process indicated by the hashed areas. This also holds for the rest of the observation but is only shown close to the power plant. Compared to Fig. 9 and Fig. 11 the flight altitude is significantly lower, therefore the pixels are smaller here. An overlay to a Google Earth map is shown in the lower panel.

Airborne imaging DOAS

K.-P. Heue et al.

Title Page

Abstract

Introduction

Conclusions

References

Tables

Figures

◀

▶

◀

▶

Back

Close

Full Screen / Esc

Printer-friendly Version

Interactive Discussion



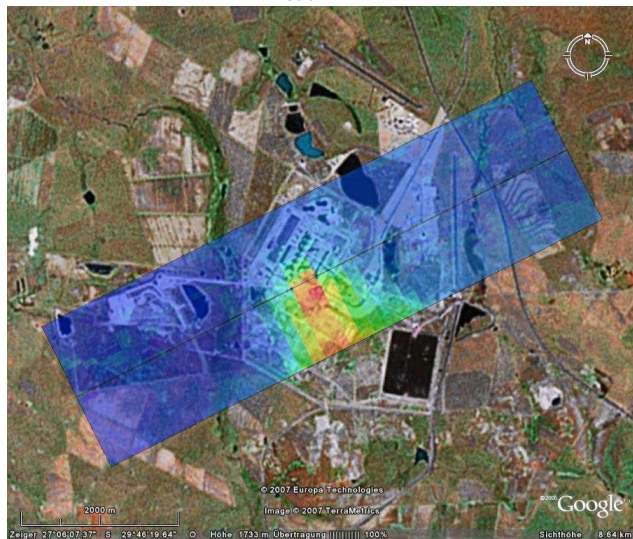
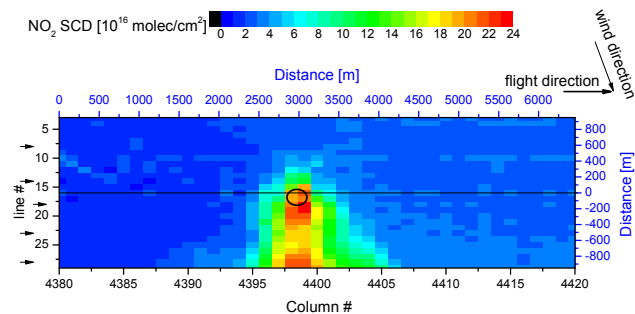


Fig. 11. NO₂ SCD (top) around the Majuba power plant (5 October 2006) overlay over a local map (bottom). Same flight level as Fig. 9, hence the pixels are wide again and the gaps are not shown. The arrows in the top figure indicate the position of the respective cross sections shown in Fig. 12. The circle shows the approximate position of the plant.

Airborne imaging DOAS

K.-P. Heue et al.

Title Page

Abstract

Introduction

Conclusions

References

Tables

Figures

◀

▶

◀

▶

Back

Close

Full Screen / Esc

Printer-friendly Version

Interactive Discussion



Airborne imaging
DOAS

K.-P. Heue et al.

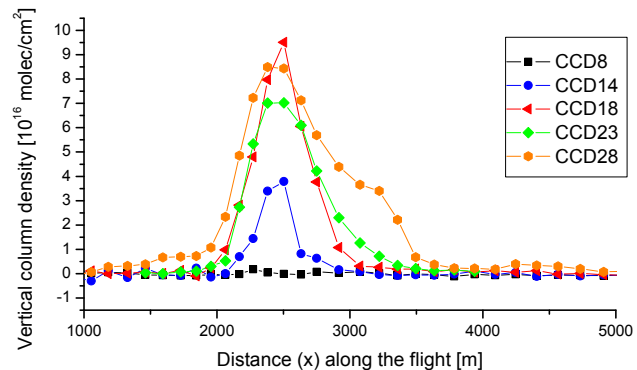


Fig. 12. Cross sections through the plume along the flight direction. The respective line are indicated in Fig. 11.

[Title Page](#)[Abstract](#)[Introduction](#)[Conclusions](#)[References](#)[Tables](#)[Figures](#)[I◀](#)[▶I](#)[◀](#)[▶](#)[Back](#)[Close](#)[Full Screen / Esc](#)[Printer-friendly Version](#)[Interactive Discussion](#)

Airborne imaging
DOAS

K.-P. Heue et al.

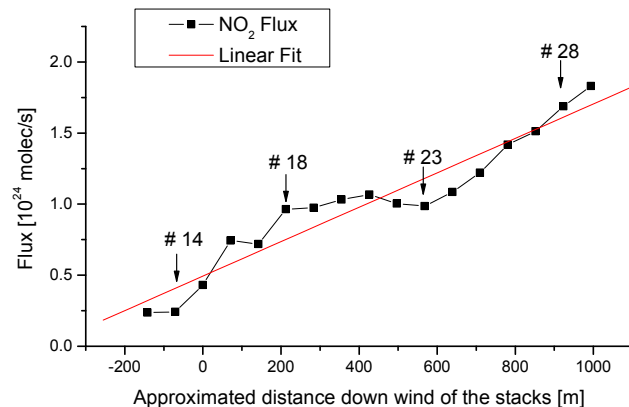


Fig. 13. NO_2 flux downwind of the Majuba power plant. Upwind of the stack the NO_2 columns are slightly enhanced. Perhaps the positions of the stacks are not known precisely enough or the low wind speeds allows some turbulent mixing close to the buildings.

[Title Page](#)[Abstract](#)[Introduction](#)[Conclusions](#)[References](#)[Tables](#)[Figures](#)[I◀](#)[▶I](#)[◀](#)[▶](#)[Back](#)[Close](#)[Full Screen / Esc](#)[Printer-friendly Version](#)[Interactive Discussion](#)

Airborne imaging
DOAS

K.-P. Heue et al.

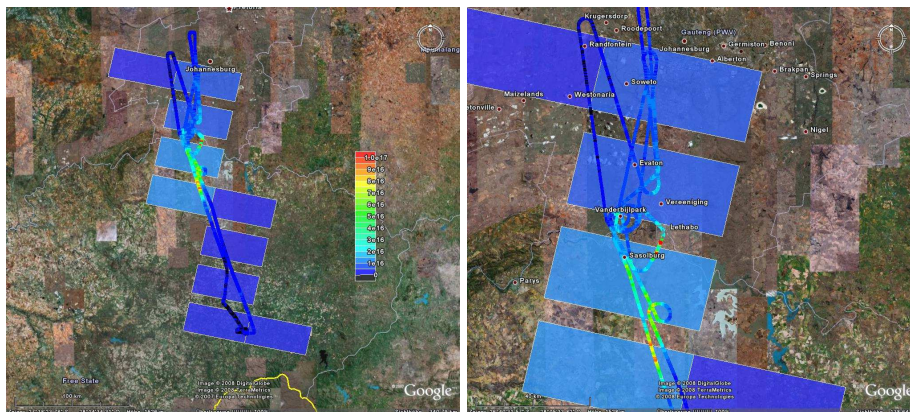


Fig. 14. Comparison between SCIAMACHY tropospheric SCD (Beirle et al., 2006) and the averaged iDOAS column density data from 6 October 2006. Strongly enhanced column densities were observed by the Imaging DOAS instrument in the industrial area around Vereeniging. Due to the large sampling area of SCIAMACHY the local enhancement affect the satellite observations only slightly.

Title Page

Abstract

Introduction

Conclusions

References

Tables

Figures

◀

▶

◀

▶

Back

Close

Full Screen / Esc

Printer-friendly Version

Interactive Discussion

